ISIJ International, Vol. 52 (2012), No. 9, pp. 1698–1704

Phase Evolution, Microstructure and Hardness of TiB_2-based Co-containing Composite by SHS under Pseudo-isostatic Pressure

Marta ZIEMNICKA-SYLWESTER,* Kiyotaka MATSUURA and Munekazu OHNO

Division of Materials Science and Engineering, Faculty of Engineering, Hokkaido University, Sapporo, Hokkaido, 060-8628 Japan.

(*Received on February 7, 2012; accepted on April 10, 2012*)

TiB_2-based cermets with various Co contents were fabricated from elemental powders "in situ" by means of the Self-propagating High-temperature Synthesis, SHS, and Pseudo- Hot Isostatic Pressing, P-HIP method. The sample pressed into a cylindrical compact was ignited in a steel can by an external heating element coiling the can. After SHS initiation, which was detected by rapid temperature increase, the samples were quickly pressed pseudo-isostatically under a pressure of 192 MPa and held for 5 min. Samples with predominant concentration of TiB_2, which varied from 70 to 85 vol.% with the addition of 5 vol% of Ti, were investigated in this study. Appreciable differences in terms of microstructure, density and hardness were observed depending on the composition. The average TiB_2 grain size increased while porosity decreased with rising concentration of TiB_2. The material synthesized with increased to 85% concentration of superhard TiB_2 grains and minimized concentration of Co exhibited greatest densification, highest hardness of about 2 400 HV, and the most homogenous microstructure. The reaction mechanism was reportedly proposed, based on temperature monitoring during combustion and previously reported references.

KEY WORDS: TiB_2; Co; SHS; P-HIP; superhard materials; microstructure.

1. Introduction

TiB_2-based composites have undergone extensive development over the past few decades stimulated by their unique properties, such as high strength-to-density ratio,[1)] good fracture toughness, inertness during machining and excellent corrosion resistance maintained at elevated temperatures.[2)] TiB_2-based materials have received wide attention not only because of their extremely high hardness in comparison to other representatives of superhard materials,[3)] but also due to their superior thermal and electrical conductivities.[4)] Therefore, the potential applications include cutting tools, space craft,[5)] and high temperature structural materials.

Apparently, WC-based Co-bonded hard cermets are most widely used for similar applications.[6)] However, shortage of tungsten and relatively low corrosion resistance of WC-based cermets restrict application of those hard composites.[7,8)] For this reason, so-called tungsten free hard metals, such as TiB_2, have been developed and introduced in industry.[9,10)]

Despite those useful properties of TiB_2, the application of monolithic TiB_2 is limited due to its poor sinterability, caused by the strong covalent bonding.[4)] Special sintering techniques such as Hot Isostatic Pressing, HIP, can achieve relatively high densification of TiB_2.[1,11)] However, HIP requires large energy consumption from external heating element. In order to simplify consolidation, sintering process can be simplified by introduction of some additives, for example binder phase in cermets. It was reported that spark plasma sintering, SPS, is a convenient and rapid method for fabrication of TiB_2–Ni,[12)] however it is also an energy consuming technique. Contrary to that, Self-propagating High-Temperature Synthesis, SHS can reduce external heat needed for sintering by utilizing heat released during highly exothermic synthesis reactions. The reaction of Ti and B is characterized by a high exothermicity because the formation enthalpy of TiB_2 from elements is as large as 76 kcal/mol so that the adiabatic temperature T_{ad} may attain a value of 3 200 K. Economically justified method may be SHS combined with HIP.[1,13)] This rapid reaction taking place "in situ" simplifies the process by directly connecting synthesis and sintering without milling of the synthesis product to obtain sinterable powders. These two processes in one device were reported to be successfully used for TiC-based composites[10,14)] and TiB_2-based composites with low melting point binders such as Al, FeAl, Cu.[6,14–18)]

However, despite many advantages of the SHS such as applicability to synthesis of unique compounds or composites, it is difficult to control this process and to study the mechanism of reaction.[19,20)] Such process is characterized by extremely high heating rates (up to 10^6 K/s), high temperature (up to 3 200 K for TiB_2) and short time of reaction completion (usually less than 1 s, sometimes even 10^{-3} – 10^{-2} s). The mechanism and kinetics of SHS as well as the combus-

* Corresponding author: E-mail: marta.zs@eng.hokudai.ac.jp
DOI: http://dx.doi.org/10.2355/isijinternational.52.1698

tion wave propagation rate depend on many physico-chemical features of a reacting mixture in any particular case. Of great significance here are the dispersion and morphology of initial powders, the homogeneity and porosity of their mixture, the presence of chemical admixtures and gases adsorbed in reactants.[21,22] Under typical conditions, for Ti powder dimensions of about 10 μm reaction front velocity is Uc ~1 cm/s, the reaction front travels the distance of one grain in ~10^{-3} s.[23] Moreover, the SHS theory predicts loss of stability when the specific heat of reaction decreases or heat loss increases causing stable SHS impossible, and then the reaction front cannot propagate with constant velocity.[20] Indeed, the explanation of reactions mechanism for Ti–B–Co system is difficult and challenging, and it has not been determined or not reported yet.

The most widely studied SHS has been reported for TiC as a refractory and abrasive material (Prokudina *et al*., Shkiro and Borovinskaya, Merzhanov *et al*.) as well as more currently Holt and Dunmead.[24] The reaction mechanism was also reported by Munir and Tamburini.[21] However, only several papers describe the reaction of Ti and B which is also highly exothermic.[2] Theoretically, the adiabatic combustion temperature T_{ad} of 3 190 K[25] is slightly lower than the melting point for TiB_2. A. S. Shteinberg and V. A. Knyazik reported that reaction of B and Ti proceeds at a noticeable rate long before the titanium melting.[22] According to B. B. Khina,[25] such diffusion controlled reaction mechanism is of great significance especially for thermal explosion mode, because of relatively low heating rate before ignition.

It is expected that boron reacts with titanium and TiB nearby TiB_2 are produced releasing heat of strongly exothermic reaction at the same time.

In assessing the comprehensiveness of a detailed reaction mechanism, the relevant question to ask is whether the mechanism can describe all classes of combustion phenomena over all possible ranges of thermodynamic and system parametric variations. Since the product of an elementary reaction depends on the energetics, its effect at the macroscopic level is mainly manifested through the temperature but also the concentration of components.[26] Indeed, for characterization of the processes sequence, a comprehensive study must include extensive and possibly independent variation of ignition and flame temperature, system pressure and reactants concentration.[26] In this study, the capabilities of detections are significantly limited because of pressure conditions in P-HIP device, also the thermal conditions significantly deviate from adiabatic. The reaction mechanism during SHS for ternary Ti–B–Co system was not reported, indeed the most probable mechanism was proposed reportedly, based on temperature monitoring during combustion, phase composition, thermodynamic data, phase equilibrium diagrams and previously published proposed SHS mechanisms.

The present paper describes attempts to obtain bulk TiB_2-based materials, using SHS combined with Pseudo- Hot Isostatic Pressing, P-HIP. This paper is focused on the consolidation, TiB_2 grains size and their distribution for TiB_2-based composites for Ti–B–Co system.[27] It can be expected that the hardness of TiB_2-based composites would be reduced by additives such as Co. In order to ensure high hardness of investigated composites, which is required for cutting tools, the concentration of Co was essentially reduced only to improve the consolidation process.

2. Experimental

2.1. "Green" Samples

The experiments described in this paper were carried out with four TiB_2-based composites, prepared from commercial elemental powders, such as titanium (45 μm, 95%), amorphous boron (0.8 μm, 95–97%), and cobalt (1.3 μm, 98%). In order to complete the boron conversion during such rapid SHS reaction, titanium and boron were set in nonstoichiometric ratio, the concentration of titanium exceeded the amount corresponding to TiB_2 formation. Each time the excess Ti-addition corresponded to 5 vol.% the "green compacts", while the Ti:B weight ratio equaled 2.402; 2.414; 2.428; 2.443 respectively. The intended concentration of TiB_2 after SHS varied from 70 to 85 vol.%. Those "green samples" contained respectively 17.95; 25.79; 32.99; 39.63 mass% of Co which correspond to 10, 15, 20 or 25 vol% of Co in "green compact". The powders were mixed for 5 h in 30 minutes cycles in laboratory rotary mill with the addition of acetone in small plastic containers, using a combination of small (5 mm in diameter) and big (10 mm) ZrO_2-milling balls. Afterward, acetone was partially evaporated on a heating plate at 343 K and then the powders were dried for 2 h in a vacuum furnace at 673 K. The powders were pressed in a steel die into a compact of 30 mm in diameter and 30 mm in thickness under a pressure of 566 MPa and then were dried again at the same conditions as those described above. The compacts were covered with a protective graphite sheet, then inserted into a vacuum chamber and closed in a steel can. In order to ensure high vacuum atmosphere inside the can, the air was pumped out from the vacuum chamber for 40 min and then can was closed under a pressure of 176 MPa in the vacuum chamber.

2.2. The SHS-P-HIP Device and Process Parameters

Samples were simultaneously synthesized and sintered using the P-HIP method in a vacuum furnace; SHS was applied for chemical reaction and to supply additional heat for sintering. The main part of the experimental device, which is situated in a vacuum chamber and put on a pressing machine, is schematically illustrated in **Fig. 1**. A press mould made of steel S45C was covered with a heat-insulating glass wool, while the bottom and top of mould rammers were separated with paperboards. Dried sand was used as both a pressing medium and electrical insulator. In order to ensure a high vacuum level of 10 Pa, the air was pumped out for 1 hour before experiment. Then steel can with sample was heated with a rate of 20 K/min, using alternating voltage, to the ignition temperature of the SHS reaction. The onset of the SHS reaction was recognizable by sudden and rapid temperature rise. The temperature of the bottom of the steel can covering the "green sample" was measured using a type-K thermocouple.

When the onset of the SHS reaction was detected, pressure was increased from an initial value of 30–35 MPa to 192 MPa and held for 5 min. Samples were taken out after cooling below 373 K.

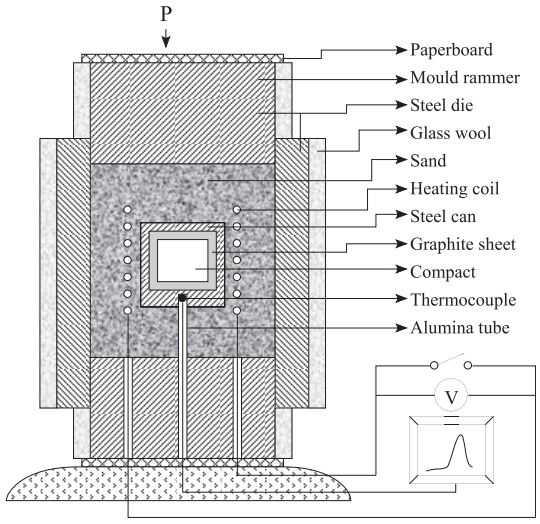

Fig. 1. Scheme of pressed mould set for SHS-P-HIP process.

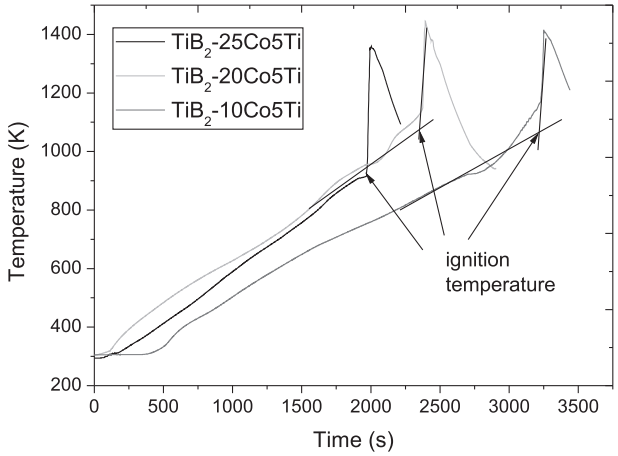

Fig. 2. Temperature profile during SHS-P-HIP process for samples with changeable concentration of Co (measured for steel can bottom).

2.3. Materials Characterization

The SHS products were cross-sectioned with diamond wheels and polished with diamond dispersive finishing with 1 μm. The phase compositions of products were determined using an X-ray Diffractometer, XRD, combined with Rietveld methods.[28,29] A Field Emission Scanning Electron Microscope, FE-SEM, and an Electron Probe Micro-Analyzer, EPMA, were applied to characterize the microstructure of the synthesized composites. A Wavelength Dispersive X-ray, WDS, analyzer was used for phase indentation. The approximate relative density was measured using volume fraction of porosity determined with a planimetric method while working on a High Resolution Optical Microscopy, HR-OM image. In order to measure apparent density Archimedes method was applied using ethanol as a liquid medium. The Vickers hardness $HV_{1.0}$ and Vickers microhardness μHV_{100}, were measured.[30,31]

3. Results and Discussion

3.1. Temperature-time Profile of SHS-PHIP Process

The temperature-time profiles for samples with various concentrations of TiB_2, measured in the bottom of the steel can covering the sample, are shown in **Fig. 2**.

That heating rate was approximately 20 K/min during the initial stage. When the temperature reached about 1 000 K, the rapid temperature increase, indicating the ignition of SHS, was observed. The ignition temperature and expected maximum temperature caused by SHS should be much higher, according to the adiabatic temperature; however that process was not carried out in adiabatic conditions. Also, the temperature profile was monitored in the steel can, outside the sample. The heating rate was slightly changed before that sudden increase, which means that some exothermic reactions took place at lower temperatures. According to an equilibrium phase diagram for Ti–Co system and references the reaction between these elements perhaps started with intermetallics formation, and then TiCo was formed.[32,33] Such weakly exothermic synthesis, much less exothermic than for boride,[32] may have released some heat initiating the SHS reaction for TiB_2 formation.

The intrinsically fast reaction velocity and elevated temperature of the SHS reaction limited the investigation on the reaction mechanism. Moreover, the SHS reaction conditions (raw powders consolidated as a compact and closed in a steel can) and high pressure in P-HIP process were not convenient to interrupt the reaction propagation. Indeed, the predicted mechanism of conversion from the elemental starting powders (Ti, B, and Co) to the final materials is described reportedly based on XRD pattern, microstructure, equilibrium phase diagrams, thermodynamic data and references. Apparently, the reaction mechanism for Ti–B–Co system in SHS process has been not reported yet.

The mechanism of phase evolution from elemental powders to SHS products should be strongly affected by average grain size of starting powders, especially Ti, and heating rate before ignition.[21,25] The TiB_2 formation mechanism is expected to be variable; starting with primary TiB_2 formation by means of solid-state diffusion-controlled phase formation kinetics and finished with dissolution-precipitation rote process. According to B. B. Khina,[25] in compounds constituted by smaller atoms such as nitrides, carbides and many borides, the partial diffusion coefficient of the small nonmetal elements exceeds that of metal atoms by several orders of magnitude, which is due to the interstitial diffusion mechanism. Hence, the growth of titanium diboride occurs at the Ti/TiB_2 or Ti/TiB interface and it is controlled by the diffusion of boron atoms across the TiB_2 layer. Such highly exothermic reaction of TiB or TiB_2 formation causes melting of Co, unreacted Ti and solid solutions which were formed during heating of compact before SHS reaction. The Co–B system consists of three binary compounds – Co_3B, Co_2B and CoB and the terminal solid solutions. The incongruently melting phase Co_3B with peritectic temperature of 1 125°C and eutectic temperature of 1 110°C is lower than maximal temperature recorded for steel can covering the sample. Also the Co–Ti phase equilibrium diagram indicates that liquid phase should be expected because of Ti_2Co formation by means peritectic reaction at 1 058°C and then eutectic point at 1 020°C.[33] Considering some temperature gradient between reacting compact and tip of thermocouple surrounded by alumina bar and being in tough with steel can covering the compact, the maximum temperature of reacting

material should attain the melting point of Co. The amount of liquid Ti is strongly affected by initial size of Ti grains in the "green compact", and heating rate to the melting temperature of the lowest melting point reactant in thermal explosion mode.

The solid-state diffusion-controlled TiB_2 growth should be expected as a predominant mechanism for heating rate 20 K/min (0.33 K/s) and Ti grain size 45 μm, considering the phase formation mechanism explained by B. B. Khina.[25] Hence, sufficiently thick "shell" of the primary product can be formed on a metal-grain surface to prevent the liquid core from spreading. As a result, secondary TiB_2 formation from liquid phase occurred. It should be expected that the concentrations of liquid Co and unreacted Ti determine quantitatively the existence of secondary TiB_2 crystalized from liquid phase. Finally, the solidification of $Ti_3Co_5B_2$, as the lowest melting point compound in Ti–B–Co system can be expected.[27]

To summarize, the proposed mechanism for Ti–B–Co system is based first of all on TiCo, TiB formation, followed by TiB_2 formation and accompanying strong heat effect. The elevated temperature caused melting of Co, unreacted Ti or intermetallic compound. Then, some primarily formed TiB_2 and unreacted graphite were partially dissolved in Co-rich liquid phase. Some secondary TiB_2 could be crystallized from liquid phase as fine grains. Afterward, the ternary compounds $Ti_3Co_5B_2$ and $Ti_2Co_{21}B_6$ can be formed at lower temperature. The combustion mechanism for experiments carried out in this study is not parallel to cermets sintered with Al[34,35] because for systems with Al the liquid phase occurs at much lower temperature at about 873 K.[36,37]

Also in the TiC system a transition from solid-diffusion to solution-precipitation controlled process detected by a change in the activation energy of SHS synthesis has been found.[38] Moreover, Munir and Anselmi-Tamburini reported[21] more quantitatively that the significance of the role played by each of these two modes is dependent on the grain size of the metal. According to theoretical calculations, the diffusion-controlled mode is dominant for Ti–C system with small metallic grains. The dominance of capillary spreading in the mechanism of SHS requires fairly large metallic grains. The capillary spreading should dominate only if the Ti powder grains exceeded 3×10^4 μm (3 cm), even if the carbon grain size is as small as 1 μm.[21] This suggests the diffusion-controlled mechanism in typical conditions, which should be expected also for Ti–B system.

The ignition temperature and maximum recorded temperature reached after the ignition observed for TiB_2–10Co–5Ti and TiB_2–20Co–5Ti samples were similar, while both ignition temperature and maximal temperature recorded for TiB_2–25Co–5Ti were about 100 K lower than those for other samples. This is not at all surprising since the adiabatic temperature for TiB_2 formation is over 3 200 K. That is why maximum temperature obtained for that reaction depends on the TiB_2 volume fraction. Therefore, increase in Co concentration reduced the maximum temperature of that process.

3.2. Phase Constituents and Microstructure of SHS-P-HIP Products

According to the XRD pattern, TiB_2 was a predominant phase in all samples, with a certain amount of $Ti_3Co_5B_2$ ternary compound (**Fig. 3**). In some cases, such as Co-rich clusters, the $Ti_3Co_5B_2$ phase was in equilibrium with negligible amount of other phase, however the amount of that phase was too small for identification using XRD. According to EDS analysis and Co–Ti–B ternary phase equilibrium diagram, such Co-rich phase correspond to $Ti_2Co_{21}B_6$. Smaller bending strength and fracture toughness should be expected for composites with intermetallic comparing to cermets such as TiB_2 with ductile, metallic Co-matrix. However, intermetallic NiAl binder seemed to be advantageous phase for TiC-based composites, and as high bending strength as 670 MPa were reported by Gao *et al*.[28,35]

Phase compositions for as-reacted materials approximately evaluated using X-ray diffraction and Rietveld method[28,29] are shown in **Table 1**. The apparent and relative densities for the samples as well as hardness are also shown in Table 1.

High values of relative density of approximately 93–98% in Table 1 were confirmed by using both Archimedes and the planimetric method. The materials with the best consolidation (relative density exceeding 97%) could be under consideration for cutting tools.

Figure 4 shows the scanning electron micrographs (SEI

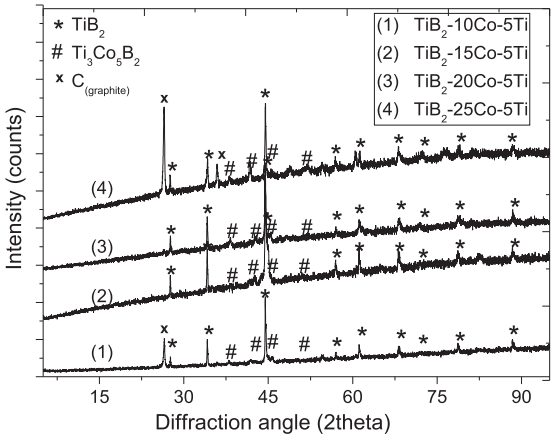

Fig. 3. The XRD pattern for TiB_2–xCo–5Ti with changeable concentration of Co.

Table 1. Physical and structural characterization of investigated samples.

Sample	Apparent density Archimedes method [g/cm^3]	Relative density planimetric method [%]	Phase composition Rietveld's method [vol.%]	Hardness Vickers's method [kg/mm^2]
TiB_2–25Co–5Ti	5.81	93.0	TiB_2 (65), Ti_3CoB_2 (23), C (12)	1 687.8 ± 358.2
TiB_2–20Co–5Ti	5.50	95.5	TiB_2 (77), $Ti_3Co_5B_2$ (23)	1 774.6 ± 345.4
TiB_2–15Co–5Ti	5.61	95.0	TiB_2 (87) $Ti_3Co_5B_2$ (13)	2 218.0 ± 691.8
TiB_2–10Co–5Ti	5.20	96.9	TiB_2 (88), $Ti_3Co_5B_2$ (9), C (3)	2 395.1 ± 355.6

with high magnifications) of cross-sectioned samples after SHS-P-HIP process. According to the WDS analysis the dark grey grains correspond to TiB_2 and grey phase surrounding these grains practically consists of Co-based $Ti_3Co_5B_2$ ternary compound in all the cases. The TiB_2 grains do not form agglomerates and are embedded in nearly continuous matrix. Relatively small pores are observed mostly on the interface between the grain and binder phase. The most homogenous and uniform microstructure indicating the best consolidation among those samples was observed for sample TiB_2–10Co–5Ti, which also exhibits the highest amount of TiB_2 content. The existence of Co is responsible for second-stage reaction mechanism in liquid phase, which is dissolution-precipitation. The reaction rate and heat effect is reduced comparing to solid-diffusion reaction. Such liquid phase is disadvantageous for consolidation process because the precipitation during solidification depends on the cooling rate. This effect caused that sample with reduced Co content revealed the best densification and the smoothest microstructure.

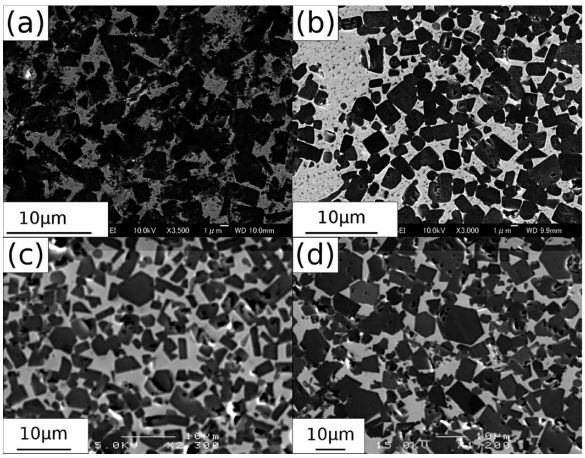

Fig. 4. SEI microstructure of samples containing various concentration of TiB_2 and Co: a) TiB_2–25Co–5Ti, b) TiB_2–20Co–5Ti , c) TiB_2–15Co–5Ti, d) TiB_2–10Co–5Ti.

Figure 5 shows the histograms for TiB_2 grain size distribution. The increase in TiB_2 content, from 70 to 85% causes that most frequently observed grain size shifts monotonically to higher values. The monomodal distribution of grain size was observed for each sample. The histograms are log-normal similar to Gaussian distribution, with exception of small grains which are ordinarily difficult to be counted. However, the largest spread for grain size distribution was recorded for sample with the highest TiB_2 concentration. Apparently, the spread also increases monotonically with increasing TiB_2 content. This effect was caused by highest heat effect and perhaps the largest maximum temperature after highly exothermic TiB_2 formation. As a result, in sample with maximum concentration of (85%) TiB_2 the biggest grain growth occurred. The crystallization of secondary TiB_2 formed from Co-rich liquid during cooling caused more fine grains, so finally the grain size distribution was more spread out. Since the melting point of Co is 1 768 K, and the lowest melting point for Ti–Co system (1 293 K)[33,39] is relatively high comparing to recorded combustion temperature, the time of crystallization from liquid phase should be relatively short.

The average TiB_2 grains size and the median (intermediate value) also increased with the increase in the volume fraction of TiB_2, as shown in **Fig. 6**. The approximated average diameter increased from 1.3 to over 4.7 μm as the TiB_2 volume fraction increased from 70 to 85%. The most significant rise in average grain size was recorded after increase in boride content from 80 to 85%. During cooling after SHS reaction the process brings about the formation of final microstructure of the product, such as Ostwald ripening and recrystallization. Since the amount of Co-based liquid was reduced the concentration of unreacted Ti and B in the liquid phase increased so the liquid solution was more saturated for recrystallization and grain growth. Also higher combustion temperature could affect the growth of the TiB_2 grains. The SHS reaction for samples with reduced Co concentra-

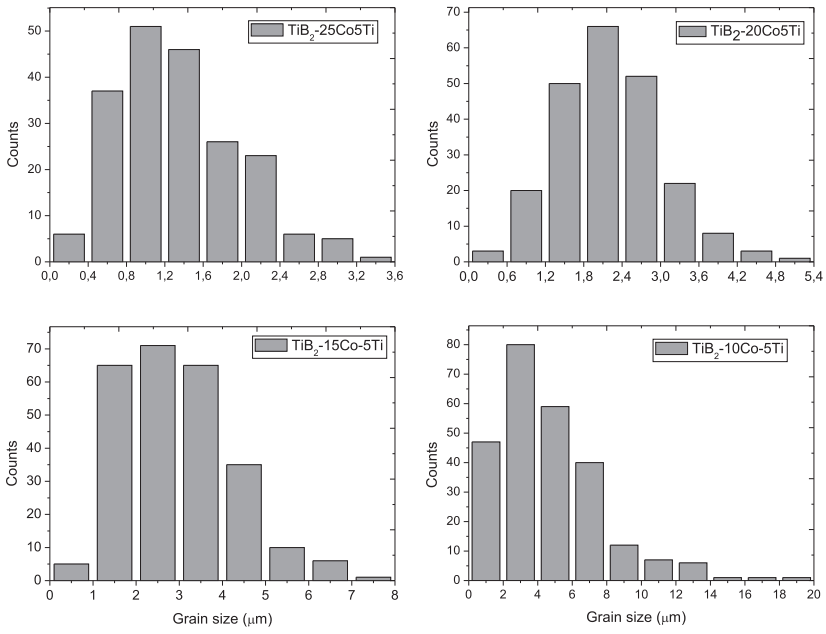

Fig. 5. Histograms indicating the grain size distribution for investigated samples.

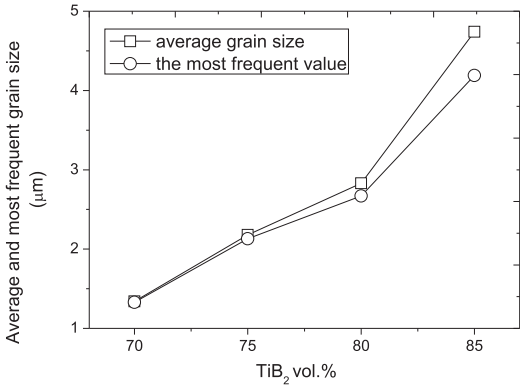

Fig. 6. Average grain size and the most frequent grain size for TiB_2-based composites with various concentration of TiB_2.

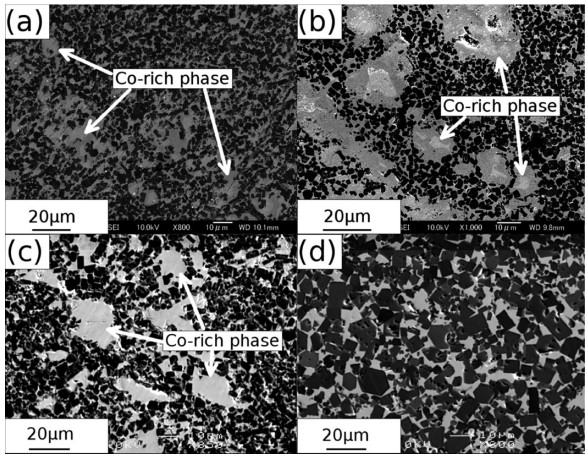

Fig. 7. The SEI image with low magnification of sample: a) TiB_2–25Co–5Ti; b) TiB_2–20Co–5Ti, c) TiB_2–15Co–5Ti, d) TiB_2–10Co–5Ti.

tion caused more elevated maximum temperature. It can be explained by adiabatic temperature, which is much higher for TiB_2 than for TiCo or other intermetallic formation. Such higher temperature caused more significant grain growth, observed in the microstructure.

Even if the SHS is characterized by non-equilibrium conditions, the effects of formation of intermetallic instead of metal binder can be explained by phase equilibrium in Ti–Co–B system.[27] Since the ternary compound $Ti_3Co_5B_2$ appears in the system, the existence of Co phase as a binder is impossible for equilibrium conditions. Similar processes were reported previously for Ti–Ni–C system.[10,40]

According to XRD patterns (Table 1), graphite inclusions were also distinguished in samples with the lowest and the highest Co content. That carbon contamination perhaps originated from the graphite sheet covering "green compact", which was partially dissolved in Co-based liquid phase after SHS reactions. Such grains are visible in the microstructure as the small black inclusions in the binder phases (Figs. 4(a), 4(d)). Sample TiB_2–10Co–5Ti exhibited the highest temperature after SHS caused by the highest concentration of TiB_2. This high temperature implicated solubility and diffusion of carbon from graphite sheet covering sample. Sample with the lowest TiB_2 content perhaps contained the highest volume fraction of Co-rich liquid phase after SHS for TiB_2 formation, so graphite could be soluble.

The maximum temperature measured for steel can covering the green sample was above 1 423 K. It is expected that local temperature within the compact was higher after the SHS reaction. The lowest melting point of 1 293 K for some intermetallic compounds in Ti–Co system[39,33] or less than 1 073 K for ternary compounds[27,41] indicates that liquid phase must have occurred after the SHS reaction causing highly exothermic effect. Such existence of carbon in a binder phase could be explained by partial solubility of graphite sheet in a cobalt-based liquid phase, originated from melting of cobalt after exothermic TiB_2 formation.

3.3. Homogeneity

In order to investigate the homogeneity of samples, SEI micrographs with a lower magnification were analyzed (**Fig. 7**.). Each above microstructure image with the low magnification indicates that homogeneity of samples depended on the concentration of Co. Some Co-rich clusters consisting of $Ti_3Co_5B_2$ and negligible amount of $Ti_2Co_{21}B_6$ could be observed in the microstructure, however after reduction of Co content to 10% (Fig. 7(d)), that Co-rich clusters disappeared and sample exhibited more homogenous microstructure.

Porosity is also less visible in the sample with the lowest Co content which confirmed the highest relative density determined with the OM image. The homogeneity and porosity depend on Co concentration since cobalt addition is of great importance as a soluble additive. As a result, Co reduces the exothermic effect caused by TiB_2 formation. Moreover, during heating some other reaction (Ti + Co, or B + Co) may occur instead of TiB_2 formation.

3.4. Hardness

In order to evaluate mechanical properties of investigated samples Vickers hardness and microhardness were determined. Moreover, the comparisons of hardness and microhardness values as well as spread of results were important factors for homogeneity consideration. That is why the hardness and microhardness were investigated for both TiB_2 grains and matrix phase and probes were repeated 42 times for each sample. Average values and uncertainty expressed as a standard deviation are shown on (**Fig. 8**) as an error bars.

Both hardness and microhardness of investigated samples monotonically increase with increasing TiB_2 grain volume fraction. That tendency was expected since TiB_2 is one of the hardest compounds and theoretically may attain microhardness of 34 GPa.[42] The spread of hardness $HV_{1.0}$ obtained experimentally were 7.42–19.62 GPa; 7.13–27.44 GPa; 13.73–28.53 GPa and 16.04–29.68 GPa for samples with 25, 20, 15 and 10 vol.% of Co respectively. Such wide distribution of results indicates that $Ti_3Co_5B_2$-based matrix essentially reduced the hardness of investigated composites. Hardness should be affected not only by the existence of superhard TiB_2 grains but also by porosity. According to that homogenous tendency, chemical composition, more than porosity, determines the hardness of investigated composites. Such tendency confirmed good densification and low porosity of investigated materials. The microhardness slightly exceeded hardness for each sample, which should be expected since hardness depends on the measurement

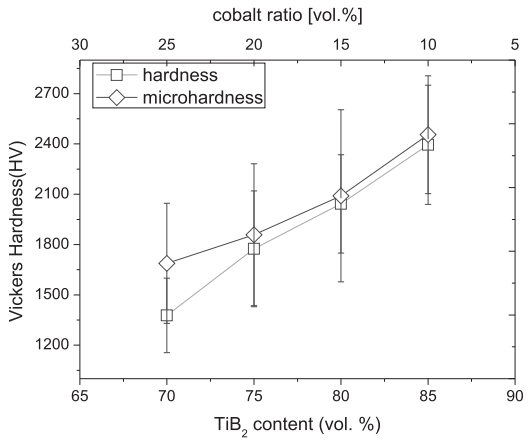

Fig. 8. Vickers hardness and microhardness for TiB_2-based composites oversaturated with Ti, with variable concentration of Co and TiB_2, uncertainty is expressed as a standard deviation (error bars).

conditions, especially loading of Vickers pyramid. However, such small reduction of hardness in terms of increased loading indicates good homogeneity and low porosity of the samples. The uncertainty for hardness distribution is smaller for sample containing the lowest Co content, which indicates the most homogenous microstructure. It indicates that reduced volume fraction of Co-rich binder improved the uniformity of the properties.

4. Conclusions

The TiB_2-based super hard composites with Co-based binder were successfully fabricated from elemental powders, using the Self-propagating High-temperature Synthesis and simultaneously sintered in a pseudo-hot isostatic pressing device. The XRD results confirmed by WDS analysis indicated that intermetallic compounds $Ti_3Co_5B_2$ was formed as a binder. The experiments carried out with a series of samples containing various Co contents indicated that increased TiB_2 volume fraction caused better densification, more homogenous microstructure and higher hardness. Each sample exhibited high hardness, which increased monotonically from 1 300 to 2 400 HV when TiB_2 increased from 75 to 85 vol.%. Moreover, relatively good consolidation with relative density of 93% to 97% was determined. The reaction mechanism of TiB_2 synthesis is suggested to be at least two-stage; starting with primary TiB_2 formation by means of solid-state diffusion-controlled process which is dominant and in a second stage, dissolution-precipitation process. Finally, the solidification of $Ti_3Co_5B_2$ was confirmed experimentally. The combustion reaction of Ti with B has completeness since the 5% of saturating Ti was applied. The most homogenous microstructure and the highest hardness, exceeding 2 380 HV, were determined for sample TiB_2–10Co–5Ti.

Acknowledgments

The authors express their appreciation for partial support by 17th ISIJ Research Promotion Grant. The authors wish to thank also for partial support received from A-STEP by JST (No. AS2211487C) and for cooperative contribution from Nihon Hard Metal Co., Ltd.

REFERENCES

1) A. Calka and D. Oleszak: *J. Alloy. Compd.*, **440** (2007), 346.
2) K. Matsuura, K. Ohsasa and Y. Obara: *Mater. Sci. Forum*, **561–565** (2007), 769.
3) K. Matsuura, Y. Hikichi, Y. Obara, T. Ohmi and M. Kudoh: *Int. J. SHS*, **4** (2005), No. 14, 305.
4) F.-C. Wang, Z.-h. Zhang, J. Luo, C. Huang and S.-K. Lee: *Compos. Sci. Technol.*, **69** (2009), 2682.
5) C. Unuvar: Combustion Synthesis for NASA's New Vision for Space Exploration, Moon, Mars & Beyond, VDM Verlag Dr. Muller, Germany, (2007).
6) K. Matsuura, Y. Obara and M. Kudoh: *ISIJ Int.*, **46** (2006), No. 6, 871.
7) G. Jiang, H. Zhuang and W. Li: *Combust. Flame*, **135** (2003), 113.
8) G. Jiang, W. Li and H. Zhuang: *Mater. Sci. Eng. A*, **354** (2003), 351.
9) I. Hussainova, J. Kubarsepp and J. Pirso: *Wear*, **250** (2001), 818.
10) X. Zhang, X. He, J. Han, W. Qu and V. L. Kvalin: *Mater. Lett.*, **56** (2002), 183.
11) W. Wang, Z. Fu, H. Wang and R. Yuan: *J. Eur. Ceram. Soc.*, **22** (2002), 1045.
12) J. Jaroszewicz and A. Michalski: *J. Eur. Ceram. Soc.*, **26** (2006), 2427.
13) A. K. Khanra, L. C. Pathak, S. K. Mishra and M. M. Godkhindi: *Mater. Lett.*, **58** (2004), 733.
14) K. Matsuura, Y. Hikichi and Y. Obara: *Adv. Sci. Tech.*, **45** (2006), 1024.
15) K. Matsuura, Y. Obara and K. Kojima: *Int. J. Refract. Met. H.*, **27** (2009), 376.
16) Y. Obara, M. Kudoh and K. Matsuura: *Mater. Trans.*, **49** (2008), No. 5, 1168.
17) K. Matsuura and Y. Obara: *Mater. Sci. Forum*, **539–543** (2007), 809.
18) Y. J. Kwon, M. Kobashi, T. Choh and N. Kanetake: *Scr. Mater.*, **50** (2004), 577.
19) L. Zhan, P. Shen and Q. Jiang: *Powder Technol.*, **205** (2011), 52.
20) A. S. Mukasyan, A. S. Rogachev and A. Varma: *Mater. Interfaces Electrochem. Phenom.*, **45** (1999), 2580.
21) Z. A. Munir and U. Anselmi-Tamburini: *Mater. Sci. Rep.*, **3** (1989), 277.
22) A. S. Shteinberg and V. A. Knyazik: *Pure Appl. Chem.*, **64** (1992), No. 7, 965.
23) A. S. Makasyan and A. S. Rogachev: *Prog. Energ. Combust. Sci.*, **34** (2008), 377.
24) S. D. Dunmead: Carbide, Nitride and Boride Materials- Synthesis and Processing, Chapter 10, Processes, ed. by A. W. Weimer and C. S. Halu, Chapman&Hall, London, (1997).
25) B. B. Khina: Combustion Synthesis of Advanced Materials, Nova Science Publishers, Inc., New York, (2010).
26) Ch. K. Law: *Proc. Combust. Inst.*, **31** (2007), 1.
27) Handbook of Ternary Alloy Phase diagrams, Vol. 5, ed. by P. Villars, A. Prince and H. Okamoto, ASM International, The Materials Information Society, USA, (1995).
28) H. M. Rietveld: *Acta Cryst.*, **22** (1967), 151.
29) H. M. Rietveld: *J. Appl. Cryst.*, **2** (1969), 65.
30) S. A. Shahdad, J. F. McCabe, S. Bull, S. Rusby and R. W. Wassel: *Dent. Mater.*, **23** (2007), 1079.
31) Ch. Ullner, A. Germak, H. L. Doussal, R. Morell, T. Reich and W. Vandermeulen: *J. Eur. Ceram. Soc.*, **21** (2001), 439.
32) V. I. Itin, A. D. Bratchikov, A. G. Merzhanov and M. Maslov: Plenum Publishing Corporation, New York, USA, (1981), 293, Translated from *Fizika Goreniya I Vzryva*, **17** (1981), 62.
33) Phase Dagrams of Binary Titanium Alloys (The Co-Ti system), by J. L. Murray, (1987).
34) G. Xiao, Q. Fan, M. Gu and Z. Jin: *Mater. Sci. Eng. A*, **425** (2006), 318.
35) X. Zhu, T. Zhang, D. Marchant and V. Morris: *J. Eur. Ceram. Soc.*, **30** (2010), 2781.
36) P. Zhu, J. C. M. Li and C. T. Liu: *Mater. Sci. Eng. A*, **329–331** (2002), 57.
37) K. Matsuura, Y. Hikichi and M. Kudoh: *Mater. Sci. Forum*, **475–479** (2005), 1605.
38) R. Pampuch: *J. de Physique IV, colloque C7, supplement au J. de Physique III*, **3** (1993), 1277.
39) G. Cacciamani, R. Ferro, I. Ansara and N. Dupin: *Intermetallics*, **8** (2000), 213.
40) J. Womg, E. M. Larson, J. B. Holt, P. A. Waide, B. Rupp and R. Frahm: *Science*, **249** (1990), 1406.
41) H. H. Stadelmaier, J.-D. Schobel and R. A. Jones: *Metall*, **21** (1967), 17.
42) Z. Zachariev: Metal, Ceramic and Polymeric Composites for Various Uses. Ch.3, New Superhard Ternary Borides in Composite Materials, InTech, Croatia, (2011), 61.